Journal of Renewable Materials

Tech Science Press

DOI: 10.32604/jrm.2023.028885

ARTICLE

Fluoride Ion Adsorption Effect and Adsorption Mechanism of Self-Supported Adsorbent Materials Based on Desulfurization Gypsum-Aluminate Cement

Xuefeng Song*, Minjuan Sun, Juan He and Lei Wang

College of Materials Science and Engineering, Xi'an University of Architecture and Technology, Xi'an, 710055, China

*Corresponding Author: Xuefeng Song. Email: songxuefeng@xauat.edu.cn

Received: 13 January 2023 Accepted: 07 March 2023 Published: 10 November 2023

ABSTRACT

The adsorption method has the advantages of low cost, high efficiency, and environmental friendliness in treating fluorinated wastewater, and the adsorbent material is the key. This study combines the inherent anion-exchange adsorption properties of layered double hydroxides (LDHs). Self-supported porous adsorbent materials loaded with AFm and AFt were prepared from a composite cementitious system consisting of calcium aluminate cement (CAC) and flue gas desulfurization gypsum (FGDG) by chemical foaming technique. The mineral composition of the adsorbent material was characterized by X-ray diffraction (XRD) and Scanning electron microscopy (SEM). Through the static adsorption experiment, the adsorption effect of the mineral composition of the adsorbent on fluoride ions was deeply analyzed, and the adsorption mechanism was revealed. XRD and SEM showed that the main hydration phases of the composite cementitious system consisting of CAC and FGDG are AFm, AFt, AH_3, and $CaSO_4{\cdot}2H_2O$. FGDG accelerates the hydration process of CAC and inhibits the transformation of AFt to AFm. The AFt content increased, and the AFm content decreased or even disappeared as the amount of FGDG increased. Static adsorption experiment results showed that AFm and AFt in adsorbent materials could significantly enhance the adsorption of fluoride ions. The adsorption of F^- in aqueous solution by PAG tends more towards monolayer adsorption with a theoretical maximum capacity of 108.70 mg/g and is similar to the measured value of 112.77 mg/g.

KEYWORDS

Flue gas desulfurization gypsum (FGDG); Calcium aluminate cement (CAC); AFm; AFt; Fluoride ions adsorption

1 Introduction

Fluorine is an essential trace element for the human body and is involved in normal metabolism [1], but excessive long-term intake of fluoride can cause dental and bone fluorosis and even cancer, brain damage, and thyroid disorders [2]. The World Health Organisation gives a standard of no more than 1.5 mg/L of fluoride in water [3]. China's Sanitary Standard for Drinking Water (GB5749-2006) stipulates that the content of fluoride in drinking water should not exceed 1.0 mg/L [4]. However, the demand for fluorine chemical products has increased sharply due to the rapid development of the integrated circuit, semiconductors, chips, solar cells, electronics, new energy industries, and so on [5–7], which resulted in the treatment of fluorinated wastewater has become a major global concern.

Currently, the main treatment technologies of fluorinated wastewater are precipitation [8], ion exchange [9,10], membrane separation [11], electrodialysis [12] and adsorption [13]. Adsorption is the most widely used because it is mature, easy to operate, and efficient. Adsorbent is the key to treating fluorinated wastewater. Activated alumina [14–17] is one of the most widely used materials for fluoride removal, with a general fluoride ion adsorption capacity of 0.8 to 2.0 mg/g, which has the disadvantage of low adsorption capacity [18]. Yang et al. [19] roasted aluminium fumarate metal-organic skeletal compounds to obtain amorphous porous layered Al_2O_3 for the removal of fluoride ions from industrial zinc sulphate solutions. The adsorption capacity was 12.05 mg/g when the adsorbent was applied at a dosage of 10 g/L. Zhang et al. [20] prepared $CaCl_2$-modified zeolites to treat fluorinated wastewater. The adsorption capacity was 1.766 mg/g at pH values of 5~7. Chen et al. [21] synthesized a new fluoride ion adsorbent ($Fe@TiO_2$) with $Ti(SO_4)_2$ and $FeSO_4$ by precipitation, the increased hydroxyl groups on the outer surface of the adsorbent facilitate the ion exchange between F^- and hydroxyl groups, so the adsorption capacity was 53.22 mg/g under optimal conditions. Besides, biosorption [22] is considered to be one of the favourable remediation techniques for fluoride removal from aqueous solutions, but there are drawbacks such as harsh living conditions of the bacteria and a long treatment process, so the application is somewhat limited.

Layered double hydroxides (LDHs) have been extensively investigated as adsorbent materials for the treatment of polluted water due to their adjustable composition of the main lamellae, interlayer anion exchangeability, and structural memory [23–25]. Cai et al. [26] synthesized a new lanthanum intercalated dihydroxide La-doped Li/Al-LDH by coprecipitation method and obtained a maximum fluoride adsorption capacity of 35.4 mg/g much higher than that of other LDHs or reported adsorbents loaded with Sarma et al. [27] synthesized Mg/Al-CO_3 layered double hydroxides (LDHs) by the urea hydrolysis method and achieved the adsorption capacity of 15.13−27.03 mg/g at 303 K. Compared with some reported adsorbents, LDHs showed better adsorption capacity and could be reused for up to five fluoride ion adsorption-desorption cycles. Teixeira et al. [28] roasted Mg-Mn-Al LDHs to treated industrial wastewater with fluoride ions at a mass concentration of 162 mg/L. The fluoride removal rate was 95.11% when the adsorbent was applied at a dosage of approximately 37.6 g/L.

Layered bimetallic hydroxides show good fluoride removal performance due to their unique structural properties [29]. However, most of the currently developed layered bimetallic hydroxides are nanoscale powders. The main problems are not gelled and not self-supporting, resulting in a large amount of fluorinated sludge in the fluoride removal process, which limits field application.

AFm ($\{Ca_4[Al(OH)_6]_2\cdot 2H_2O\}\cdot SO_4\cdot mH_2O$), AFt ($\{Ca_6[Al(OH)_6]_2\cdot 2H_2O\}\cdot (SO_4)_3\cdot nH_2O$), as the main hydration phase of Portland cement and sulfoaluminate cement [30,31], have a similar laminate structure of LDHs and exchangeable properties of interlayer anions [32]. In recent years, the preparation of adsorption and curing materials for industrial wastewater treatment with the inherent hydration phases AFm and AFt of cement-based materials and their self-gelling properties has become a hot research topic [33,34]. In this paper, based on the adsorption, exchange, and complexation mechanism of fluoride ions by conventional fluoride removal materials, a porous self-supporting fluoride ion adsorption material (Porous CAC-FGDG, PAG) was prepared by chemical foaming technique using bulk industrial solid waste flue gas desulphurization gypsum (FGDG) and calcium aluminate cement (CAC). The effect of CAC and FGDG ratio on the mineral composition (AFm, AFt, AH_3, $CaSO_4\cdot 2H_2O$) and fluoride ion adsorption capacity of PAG adsorbent materials was studied in combination with the principle of cement chemistry reaction, and the isotherm and adsorption kinetics model of PAG on fluoride ion adsorption was established.

2 Materials and Methods

2.1 Materials

CAC is CA-50 aluminate cement produced by Jianai Aluminate Cement Company, Zhengzhou, Henan Province, China. FGDG is construction gypsum (hemihydrate gypsum) prepared from flue gas desulphurization gypsum by calcination in a rotary kiln from a power plant, whose mineral composition is shown in Tables 1 and 2, respectively. The foaming agent is hydrogen peroxide (AR), purchased from Sinopharm Chemical Products Co. (China).

Table 1: Mineralogical composition (mass fraction) of CAC (w/%)

$CaO{\cdot}Al_2O_3$	$CaO{\cdot}2Al_2O_3$	$2CaO{\cdot}Al_2O_3{\cdot}SiO_2$	$4CaO{\cdot}3Al_2O_3{\cdot}SiO_2$	$CaO{\cdot}TiO_2$	$12CaO{\cdot}7Al_2O_3$	$MgO{\cdot}Al_2O_3$
51.7	10.6	27.5	1.8	5.3	0.6	2.5

Table 2: Mineral composition of FGDG (w/%)

$CaSO_4{\cdot}0.5H_2O$	$CaMg(CO_3)_2$	$K_2O{\cdot}Al_2O_3{\cdot}6SiO_2$	$CaCO_3$	Al_2O_3	Fe_2O_3	MgO
85	5.5	3.8	1.5	0.9	1.2	2.1

2.2 Preparation of PAG

CAC and FGDG with a mass ratio of 1:0, 1:0.2, 1:0.25, 1:0.4, 1:0.6, 1:0.7, 1:1, 1:1.2, 1:1.4, and 45% water (based on the mass of CAC and FGDG) were mixed to a uniform slurry using a mortar mixer, and 2% hydrogen peroxide (calculated by the sum of the masses of CAC and FGDG) was added to the slurry. After stirring at high speed for 1 min, the slurry was quickly poured into a steel mold (20 mm × 20 mm × 20 mm). Natural curing was carried out under temperature conditions of 45°C for 1 d before being demoulded to obtain the FGDG-CAC porous composite (PAG). The PAG adsorbent material was determined to have a compressive strength of 0.40–0.65 MPa, a bulk weight of 425–435 kg/m^3, an open porosity of 68%–72%, and an internal specific surface area of approximately 50 m^2/g. The specific preparation process of the PAG is shown in Fig. 1.

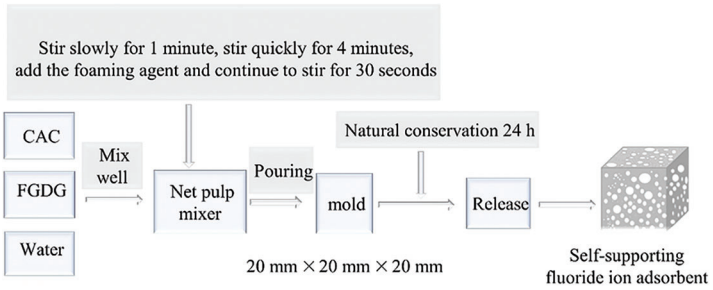

Figure 1: The specific preparation flow chart of PAG

2.3 Fluoride Ion Concentration Determination

The fluoride ion concentration in the solution was tested by a fluoride ion selective electrode (JC-PXS-F, Qingdao Juchuang Environmental Protection Group Co., Ltd., China). The sodium fluoride solution of a given concentration and a certain proportion of adsorbent were put into a conical flask and shaken at a rate of 180 r/min for 8 h, then filtered, the fluoride ion concentration of the filtrate was measured with a fluoride ion selective electrode. The optimum pH for the test is 5.0–6.0. To eliminate the interference of

Al^{3+} and Fe^{3+} in the solution to the experiment results, a citrate buffer solution is used to control the pH of the solution to be tested during the experiment.

The removal rate and adsorption capacity are calculated by Eqs. (1) and (2), respectively.

$$R(\%) = \frac{C_i - C_e}{C_i} * 100\% \tag{1}$$

$$Q_e = \frac{C_i - C_e}{m} * V \tag{2}$$

where R (%) is removal rate, C_i (mg/L) is the initial concentration of fluoride ions in solution, C_e (mg/L) is the concentration of fluoride ions at adsorption equilibrium, Q_e (mg/g) is adsorption capacity, m (g) is the amount of adsorbent and V (L) is the volume of solution.

2.4 Mineral Composition and Morphological Characteristics of PAG

The mineralogical composition of PAG was determined using an X-ray diffraction (XRD) machine (Rigaku D/max-3A, Rigaku Corporation, Japan). The microscopic morphology of PAG with different mass ratios of CAC and FGDG was observed with a scanning electron microscope (SEM; EVO 10/LS 10, Carl Zeiss, Germany).

2.5 Static Adsorption Experiment for Obtaining Effect of CAC and FGDG Mass Ratio on the Fluoride Ion Adsorption

Porous PAG adsorbent materials were prepared from composite gelling materials with CAC and FGDG at different mass ratios. The adsorbate is sodium fluoride solution with F^- concentration of 100 mg/L, and the mass ratio of PAG to adsorbate is 1:200. The PAG and adsorbate were placed in a 500 mL conical flask in a constant temperature (25°C) shaker and shaken at 180 r/min for 8 h. After filtration, the fluoride ion concentration of the filtrate was measured, and the fluoride ion adsorption capacity and adsorption efficiency were calculated.

2.6 Isothermal Model for PAG Adsorbent Adsorption

The adsorption experiment was carried out at the conditions of 25°C, pH7, the ratio of PAG (CAC and FGDG at a mass ratio 1:0.7) to adsorbate of 1:200, and different initial fluoride ion concentrations. The Langmuir and Freundlich models were used to fit the adsorption isotherm. The Langmuir isothermal adsorption equation is as in Eq. (3). The Freundlich isotherm adsorption equation is as in Eq. (4).

$$\frac{C_e}{Q_e} = \frac{1}{K_L Q_m} + \frac{1}{Q_m} C_e \tag{3}$$

where Q_e (mg/g) is the adsorption capacity per unit of adsorbent material, K_L (L/mg) is the Langmuir equilibrium constant, Q_m (mg/g) is the maximum unit adsorption capacity when the adsorption reaches saturation, and C_e (mg/L) is the mass concentration of adsorbate at adsorption equilibrium.

$$\log Q_e = \log K_F + \frac{1}{n} \log C_e \tag{4}$$

where K_F (L/mg) is the Freundlich equilibrium constant, and 1/n is the component factor reflecting the degree of difficulty of adsorption.

2.7 Kinetic Model for PAG Adsorbent Adsorption

The adsorption experiment was carried out at the conditions of 25°C, pH value is 7, the ratio of PAG (CAC and FGDG at mass ratio 1:0.7) to adsorbate of 1:200, and different initial fluoride ion

concentrations. The Quasi-first-order kinetic model and Quasi-second-order kinetic model were used to fit the absorption kinetic curves. The quasi-first-order kinetic model and quasi-second-order kinetic model are shown in Eqs. (5) and (6), respectively.

$$\ln(Q_e - Q_t) = \ln Q_e - K_1 t \tag{5}$$

$$t/Q_t = 1/K_2 Q_e^2 + t/Q_e \tag{6}$$

where Q_e (mg/g) and Q_t (mg/g) are the adsorption amount when adsorption reaches equilibrium, and After t mins of adsorption, respectively, t (min) is the adsorption time, min, and K_1 (min^{-1}) and K_2 (min^{-1}) are the adsorption rate constants.

3 Results and Discussion

3.1 Effect of CAC and FGDG Mass Ratio on the Mineral Composition of PAG

In the composite cementitious system of CAC and FGDG, according to the principle of chemical reaction of cement: firstly, the aluminate minerals (CA, CA_2) in CAC undergo a hydration reaction with water to produce CAH_{10}, C_2AH_8, and AH_3, and some of the CAH_{10} and C_2AH_8 transform into the stable C_3AH_6 with the temperature increasing. Secondly, $CaSO_4{\cdot}0.5H_2O$ in FGDG meets water to form $CaSO_4{\cdot}2H_2O$ and reacts rapidly with hydrated calcium aluminate to form AFt ($3CaO{\cdot}Al_2O_3{\cdot}3CaSO_4{\cdot}32H_2O$). When $CaSO_4{\cdot}0.5H_2O$ is insufficient, Aft converts to AFm ($3CaO{\cdot}Al_2O_3{\cdot}CaSO_4{\cdot}12H_2O$).

The hydration products of the above composite cementitious system depend on the mass ratio of CAC and FGDG. Combining the mineral composition of the two raw materials of CAC and FGDG (Tables 1 and 2), the hydration reaction equation and main hydration products under different mass ratios of CAC and FGDG were obtained by theoretical calculation, as shown in Table 3.

Table 3: Equations of hydration reactions for aluminate cement and flue gas desulfurization hemihydrate gypsum

CAC:FGDG (Mass ratio)	Reaction equation
1:0	$2CA + H \rightarrow C_2AH_8 + AH_3$
	$2CA_2 + 17H \rightarrow C_2AH_8 + 3AH_3$
≥1:0.21	$3CA + C\hat{S} + 18H \rightarrow AFm + 2AH_3$
	$3CA_2 + C\hat{S} + 27H \rightarrow AFm + 5AH_3$
≤1:0.63	$3CA + 3C\hat{S} + 37H \rightarrow AFt + 2AH_3$
	$3CA_2 + 3C\hat{S} + 46H \rightarrow AFt + 5AH_3$
	$C\hat{S} + 1.5H_2O \rightarrow CS + Q$

Note: CA is monocalcium aluminate, CA_2 is Monocalcium dialuminate, C_2AH_8 is dicalcium aluminate hydrate, AH_3 is hydrated alumina gel, AFt is trisulfide calcium sulphoaluminate hydrate, AFm is Monosulfur calcium sulphoaluminate hydrate, $C\hat{S}$ is hemihydrate gypsum, CS is dihydrate gypsum, H is water, Q is the heat of reaction.

The mineral composition and mineral morphology of the prepared porous material PAG with different mass ratios of CAC and FGDG were tested, as shown in Figs. 2 and 3, respectively.

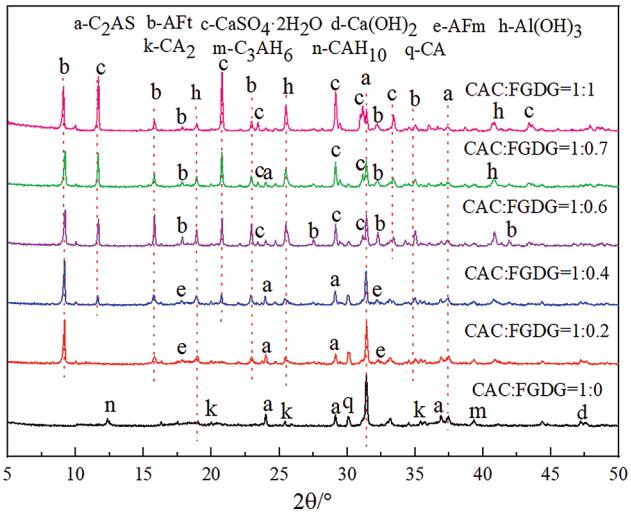

Figure 2: XRD patterns of PAG at different mass ratios of CAC and FGDG

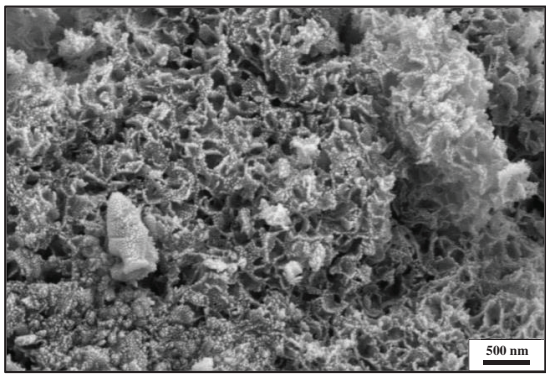

(a) CAC:FGDG=1:0.2

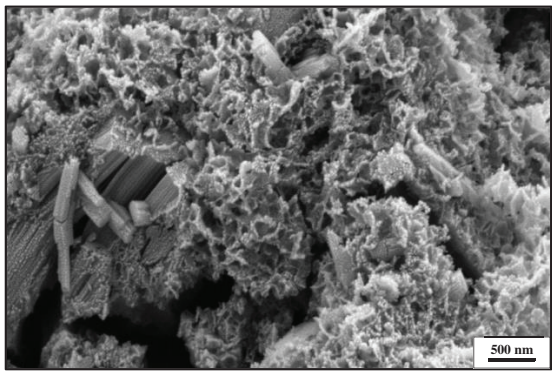

(b) CAC:FGDG=1:0.4

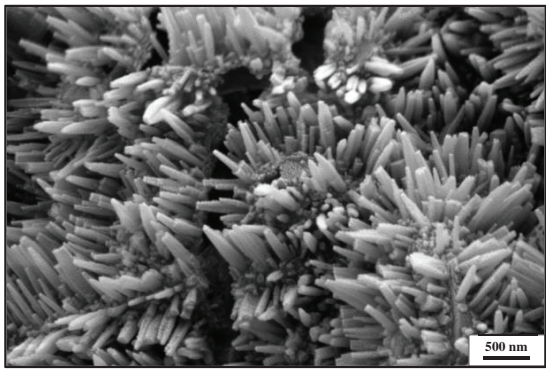

(c) CAC:FGDG=1:0.7

Figure 3: Mineral topography of PAG at different CAC to FGDG mass ratios

From Fig. 2, the following conclusions can be drawn: (1) In the pure CAC gelling system, CA and CA_2 are rapidly hydrated by water, hydrated calcium aluminates (CAH_{10}, CA_3H_6) and AH_3 were produced. At the same time, there are poorly hydrated C_2AS (PDF 73-2041, 2θ = 24.003°, 29.125°, 31.411°) and a small

amount of unhydrated CA_2 (PDF 46-1475, 2θ = 19.993°, 25.416°, 34.533°), CA (PDF 70-0134, 2θ = 30.078°, 35.398°, 44.768°). (2) In the CAC and FGDG composite gelling system, FGDG accelerates the hydration process of CAC, and the unhydrated CA and CA_2 basically disappear, while new hydration product phases AFm (PDF 50-1607, 2θ = 17.790°, 21.993°, 32.215°), AFt (PDF 41-1451, 2θ = 15.812°, 22.947°, 35.013°), and $CaSO_4{\cdot}2H_2O$ (PDF 33-0311, 2θ = 11.676°, 20.779°, 29.146°) appear. In the composite gelling system of CAC and FGDG, the diffraction peaks of the AFm phase of the hydration products weakened, and those of the AFt phase increased with the increase of FGDG doping, and the AFm phase was partially transformed into the AFt phase, and the $CaSO_4{\cdot}2H_2O$ phase was significantly enhanced.

According to Fig. 3, when the mass ratio of CAC and FGDG was 1:0.2, the main minerals of the PAG are the petal-like flake type AFm phase and the fluffy spherical particles AH_3. When the mass ratio of CAC and FGDG was 1:0.4, the main minerals of the PAG were the AFm phase with petal-like flakes, the AFt phase with needle-rod structure, and the fluffy spherical particles AH_3. When the mass ratio of CAC and FGDG was 1:0.7, the main minerals of the PAG are mainly the needle-rod AFt phase interspersed in the AH_3 gel.

3.2 Effect of CAC and FGDG Mass Ratio on the Fluoride Ion Adsorption and Analysis of the Adsorption Mechanism

From Fig. 4, the adsorption capacity and efficiency of PAG for fluoride ions tend to increase and then decrease as the mass ratio of CAC and FGDG decreases. Hydration CAC has a certain removal efficiency for fluoride ions, and its adsorption efficiency and adsorption capacity are 64.38% and 12.88 mg/g, respectively. When the mass ratio of CAC and FGDG was 1:0.2, 1:0.25, 1:0.4, 1:0.6, and 1:0.7, the adsorption efficiency of PAG on fluoride ions was 66.4%, 70.11%, 77.68%, 83.34%, and 89.56%, respectively, the adsorption capacities were 13.28, 14.02, 15.54, 16.67 and 17.91 mg/g, respectively, and the adsorption effect gradually increased with the decrease of the mass ratio of CAC and FGDG. When the mass ratio of CAC and FGDG was 1:1.0, 1:1.2, and 1:1.4, the adsorption efficiency of PAG on fluoride ions was 88.94%, 88.27%, and 84.38%, the adsorption capacity was 17.78, 17.65 and 16.87 mg/g, respectively, and the adsorption effect decreased gradually with the decrease of the mass ratio of CAC and FGDG. When the mass ratio of CAC and FGDG was 1:0.7, the adsorption effect of PAG on fluoride ions was highest.

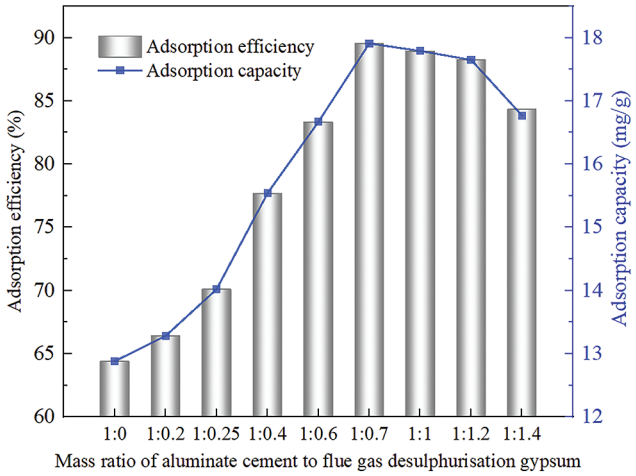

Figure 4: Effect of PAG prepared at different mass ratios of CAC and FGDG on F^- adsorption rate and adsorption capacity

Calcium salts also show excellent adsorption for the removal of fluorine, where the adsorption mechanism is mainly the adsorption of fluorine to calcium-containing adsorption sites on the surface of the adsorbent, constituting a precipitation system. Aluminate cement hydrates to produce $Al(OH)_3$ gels, which are complex to fluoride ions. Hydrotalcites (LDHs) are a class of natural, synthetic materials with good anion exchange capacity. AFm ($\{Ca_4[Al(OH)_6]_2{\cdot}2H_2O\}{\cdot}SO_4{\cdot}mH_2O$), AFt ($\{Ca_6[Al(OH)_6]_2{\cdot}2H_2O\}{\cdot}(SO_4)_3{\cdot}nH_2O$), as the main hydration phases of silicate and sulphate aluminate cements, have a similar laminate structure of LDHs and exchangeable properties of interlayer anions.

Combining the mineral composition of PAG in Fig. 2 and the fluoride ion adsorption effect of PAG in Fig. 4, the following conclusions can be drawn: (1) Hydrated AH_3, calcium aluminate hydrate (CAH_{10}, C_3AH_6), $Ca(OH)_2$ and unhydrated CA, CA_2, C_2AS existing in PAG prepared from pure CAC constitute the complexation and precipitation system of fluoride ions, and the system has certain fluoride removal function. (2) The PAG prepared by the CAC and FGDG composite system made up of AFm, AFt, $CaSO_4{\cdot}2H_2O$, and the CAC hydration products constituted a complexation, precipitation, and ion exchange adsorption system for fluoride ions, and the system exhibited higher fluoride removal efficiency. (3) Theoretically, when the CAC and FGDG mass ratio decreases from 1:0.2 to 1:0.7, the hydration phase AFm in PAG increases and then decreases, AFt increases, and AH_3 decreases, and the adsorption effect of PAG on fluorine ions gradually increases, indicating that the order of the adsorption effect of hydration phase on fluorine ions from weak to strong is AH_3, AFm, and AFt. (4) $CaSO_4{\cdot}2H_2O$ as a fluorine ion precipitant has a certain fluoride removal effect, but the excessive amount of FGDG in the CAC and FGDG composite gelling system will weaken the fluorine ion exchange adsorption effect of AFt.

To analyze the adsorption mechanism of fluoride ions by the composite gelling system of CAC and FGDG, the PAG was prepared with the mass ratio of CAC and FGDG was 1:0.4, and the mineral composition of PAG before and after adsorption of fluoride ions was determined by XRD as shown in Fig. 5.

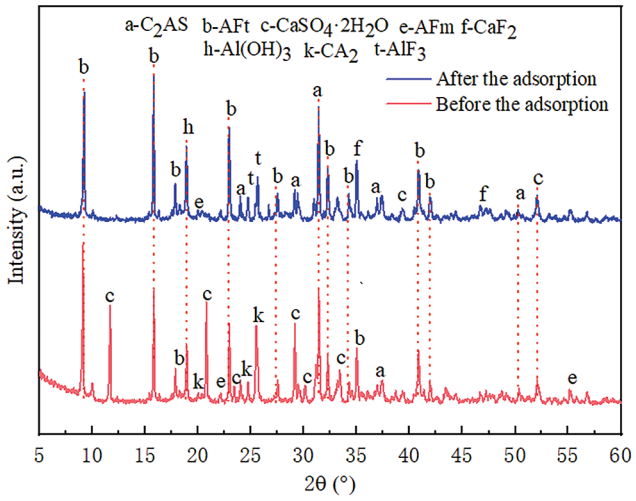

Figure 5: The phase change of PAG before and after adsorption

From Fig. 5, the following conclusions can be drawn: (1) Before the adsorption of fluoride ions, the hydrated phases in the PAG were AFm, AFt, $CaSO_4{\cdot}2H_2O$ and AH_3, which together constituted an exchange, complexation, and precipitation system for fluoride ions, in agreement with the results in Fig. 2. (2) After adsorption of fluoride ions, new fluorides CaF_2 (2θ = 34.991°, 45.336°) and AlF_3 (2θ = 25.618°) were generated in the PAG, while the main peaks of the $CaSO_4{\cdot}2H_2O$ phase largely disappeared. The characteristic peaks of the AFm and AFt phases remained largely unchanged.

The results in Fig. 5 only demonstrate the existence of the calcium ion precipitation mechanism ($CaSO_4{\cdot}2H_2O$) and the complexation adsorption mechanism of activated alumina (AH_3) for the adsorption of fluoride ions by the PAG adsorbent material prepared from the CAC and FGDG composite gelling system, which is difficult to explain the ion exchange adsorption mechanism of the AFm and AFt phases. Therefore, When the mass ratio of CAC and FGDG was 1:0.4, the elemental composition and distribution characteristics of AFm and AFt phases in PAG before and after the adsorption of fluoride ions, were determined by SEM-EDS, as shown in Figs. 6 and 7.

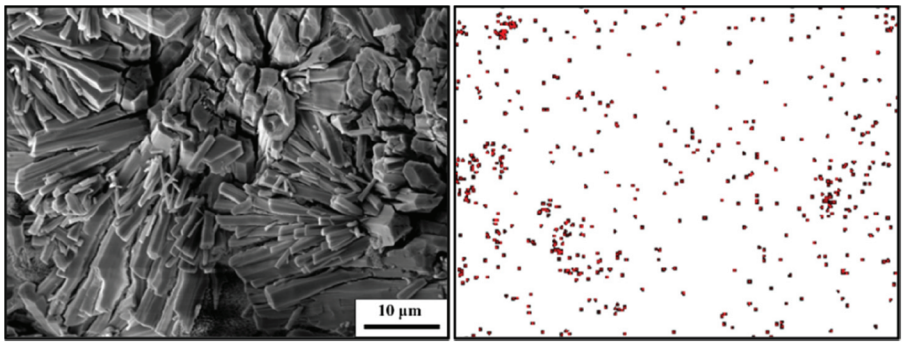

Figure 6: SEM morphology and F^- distribution of PAG after adsorbed fluoride ions

Fig. 6 shows that there were a large number of flakes AFm and short needles and rods AFt phases in the PAG composite, and the fluorine element was widely distributed in the AFm and AFt phases after treatment of fluoride-containing water samples by PAG. Fig. 7a shows that the elemental composition of the petal-like AFm phase before the adsorption of fluorine ions by PAG is O, Al, Ca, and S, which is consistent with the elemental composition of the AFm phase. After the adsorption of fluorine ions by PAG, the elemental composition of the AFm phase is O, Al, Ca, S, and F, as shown in Fig. 7a*, which proves that the fluorine ions have partially entered the AFm crystal structure and formed a new F-AFm phase through the exchange with SO_4^{2-} ions. The results in Fig. 7b show that the elemental composition of the short needle-rod AFt phase before the adsorption of fluorine ions by PAG is O, Al, Ca, and S, which is consistent with the elemental composition of the AFt phase. After the adsorption of fluorine ions by PAG, the elemental composition of the AFt phase is O, Al, Ca, S, and F, as shown in Fig. 7b*, which proves that the fluorine ions have partially entered the AFt crystal structure through exchange with SO_4^{2-} ions to form a new F-AFt phase. As for the results of the measurement, the characteristic peaks of the AFm and AFt phases before and after the adsorption of fluoride ions by the PAG remained basically unchanged, which is because the radius of the fluoride ions is much smaller than that of the SO_4^{2-} ions and the effect on their lattice parameters is not obvious after entering the AFm and AFt phases.

To further characterize the extent of exchange adsorption of AFm or AFt relative to fluoride ions, PAG (CAC and FGDG at mass ratio 1:0.2) was used as an adsorbent, deionized water (blank group) and sodium fluoride solution (experimental group) with the F^- concentration of 100 mg/L were used as adsorbate to carry out the parallel adsorption experiment at the mass ratio of PAG to adsorbate is 1:200. Choosing the mass ratio of CAC to FGDG at 1:0.2 is to minimize the influence of SO_4^{2-} released by the reaction of $CaSO_4{\cdot}2H_2O$ with fluoride ions on ion-exchange adsorption.

The exchange adsorption capacity of AFm or AFt for fluoride ions was investigated, and the results are shown in Fig. 8.

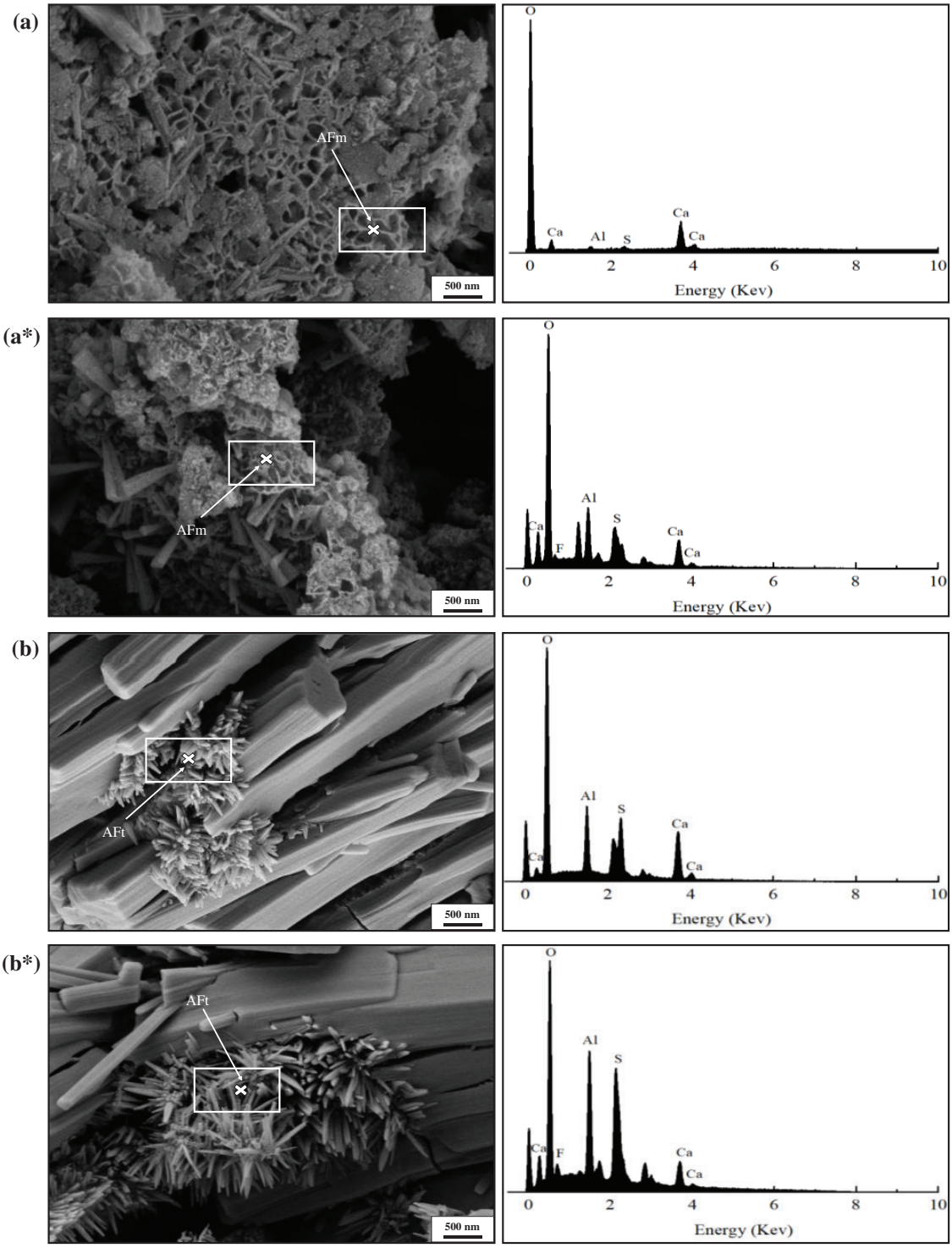

Figure 7: SEM morphology of PAG and energy spectrum point sweep before and after fluoride ion adsorption. (a) and (b) Before adsorption; (a*) and (b*) After adsorption

As shown in Fig. 8, in deionized water, the concentration of SO_4^{2-} dissolved from AFm or AFt was around 150 mg/L. In sodium fluoride solution, the concentration of SO_4^{2-} was around 210 mg/L due to the presence of ion exchange adsorption of AFm or AFt phase. So it is directly proved that PAG adsorbent material has a higher defluorination effect due to ion exchange adsorption of AFm or AFt phase. Repeated experiments were carried out to avoid chance events due to experimental errors, indicating that the data are somewhat reliable.

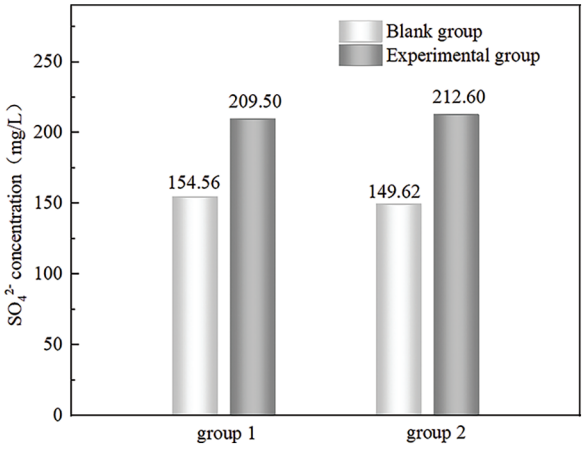

Figure 8: Changes in SO_4^{2-} concentration in solution before and after adsorption of fluoride ions by PAG

The results of the above studies showed that the PAG contains hydrated phases such as AFm, AFt, $CaSO_4{\cdot}2H_2O$, and AH_3, which achieve good fluoride removal effects through ion exchange, complexation, and precipitation mechanisms. The AFm or AFt phases significantly improve the fluoride removal effect of CAC on fluorinated wastewater through ion exchange adsorption.

3.3 PAG on F^- Adsorption Isotherms and Adsorption Kinetics

3.3.1 Isothermal Model for PAG Adsorbent Adsorption

The adsorption isotherm is often used to describe the interaction between the adsorbent and the adsorbate, and to reflect the adsorption performance of the adsorbent [35]. Commonly used adsorption isotherm models are the Langmuir model and the Freundlich model, which are based on completely uniform monolayer adsorption and heterogeneous adsorption of adsorbent, respectively [36].

The isothermal adsorption test data are shown in Table 4, the resulting fitted curves are shown in Fig. 9, and the adsorption isotherm parameters are shown in Table 5.

Table 4: F^- isothermal adsorption test data of PAG

The initial concentration (mg/L)	20	50	100	200	300	400	500	600
Equilibrium concentration C_e (mg/L)	12.82	14.68	16.08	23.10	33.19	54.62	78.48	112.77
Adsorption capacity Q_e (mg/g)	36.90	32.00	29.89	35.38	49.39	69.08	84.30	77.77
C_e/Q_e	0.35	0.46	0.54	0.65	0.67	0.79	0.93	1.45
$\log C_e$	1.108	1.167	1.206	1.364	1.521	1.737	1.895	2.052
$\log Q_e$	1.567	1.505	1.476	1.549	1.694	1.839	1.926	1.891

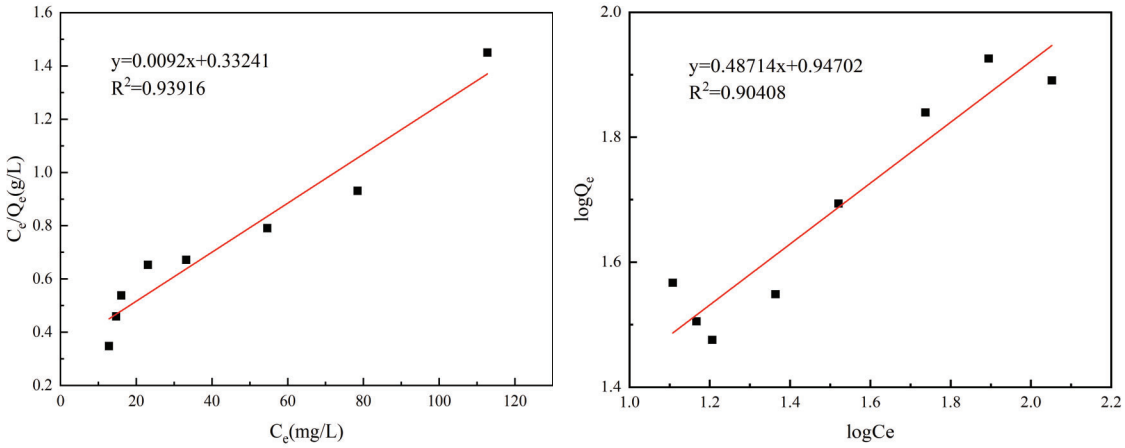

Figure 9: PAG adsorption isotherm fitting: (a) Langmuir adsorption isotherm; (b) Freundlich adsorption isotherm

Table 5: PAG adsorption isotherm parameters

Langmuir model			Freundlich model		
K_L (L/mg)	Q_m (mg/g)	R^2	K_F	1/n	R^2
0.03	108.70	0.93916	8.85	0.48714	0.90408

The Langmuir and Freundlich models were curve-fitted and the resulting fitted curves are shown in Fig. 9, and the results of the fitted parameters are expressed in Table 5. Comparing the R^2 of the fitted equations of the two adsorption models, the R^2 is 0.93916 in the Langmuir model, the R^2 is 0.90408 in the Freundlich model. The Langmuir adsorption model is a better fit than the Freundlich one, so the adsorption of F^- in an aqueous solution by PAG tends to be more like monolayer adsorption. The theoretical maximum adsorption capacity is 108.70 mg/g and is similar to the measured value of 112.77 mg/g.

3.3.2 PAG Adsorption Kinetic Model

Adsorption kinetic models are commonly used to study the various characteristics of the adsorption process. The quasi-first-order and quasi-second-order kinetic models are used to determine the liquid-solid adsorption process's controlling factors and analyze the adsorption mechanism [37]. The quasi-first-order kinetic model is suitable for describing the initial stages of the adsorption process. The quasi-second-order kinetic model describes the process of diffusion and adsorption, which is accompanied by chemical bond formation [38].

The isothermal adsorption test data are shown in Table 4, the Quasi-first-order kinetic model and Quasi-second-order kinetic model were used to fit the absorption kinetic curves, and the resulting fitted curves are shown in Fig. 10, and adsorption kinetic parameters are shown in Table 6.

As can be seen from the fitted parameters of the adsorption kinetics in Table 6, when the initial concentration of fluoride ions was 300 and 500 mg/L, the fit coefficients R^2 were all close to 1 for both the quasi-first-order kinetic model and quasi-second-order kinetic model. However, the simulated adsorption values fitted by quasi-first-order kinetic model were closer to the measured values, indicating

that most of the F^- completed adsorption on the surface of the adsorbent. A small proportion of the ions diffused into the interior of the adsorbent. The adsorption mechanism consisted of physical and chemical adsorption, but physical adsorption was more dominant. When the initial concentration of fluoride ions was 100 and 200 mg/L, the quasi-second-order kinetic model better describes the adsorption process than the quasi-first-order kinetic model. There was a large number of chemical bonds forming during the adsorption of F^- by the PAG adsorbent, so the adsorption process was dominated by chemical adsorption.

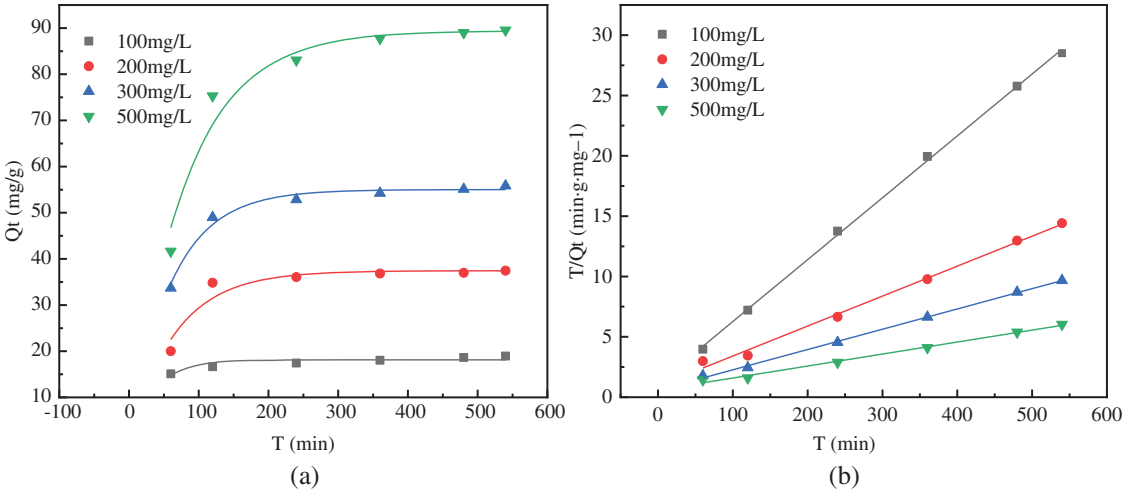

Figure 10: Fitting of PAG adsorption kinetics: (a) Quasi-first-order kinetic model; (b) Quasi-second-order kinetic model

Table 6: PAG adsorption kinetic parameters

Adsorbent concentration (mg/L)	$Q_{e,1}$ (mg/g)	Quasi-second-order kinetic model			Quasi-second-order kinetic model		
		K_1 (min^{-1})	$Q_{e,2}$ (mg/g)	R^2	K_2 (min^{-1})	$Q_{e,3}$ (mg/g)	R^2
100	18.95	0.0281	18.13	0.7244	0.0023	19.50	0.9990
200	37.44	0.0154	37.44	0.9012	0.0007	40.27	0.9933
300	55.84	0.0165	55.02	0.9802	0.0005	59.49	0.984
500	89.56	0.0123	89.41	0.9500	0.0002	100.7	0.9921

The theoretical adsorption capacity calculated by fitting the quasi-secondary kinetic equation is closer to the experimentally measured value than the calculated value from the quasi-first-order kinetic equation, and the fitted correlation coefficient is high, suggesting that the process of fluoride ion adsorption by PAG may be dominated by chemisorption. The quasi-secondary reaction kinetic model includes all processes of adsorption, such as ion exchange, membrane diffusion, surface adsorption, and intraparticle diffusion, therefore, it provides a realistic and comprehensive picture of the kinetics of fluoride ion adsorption by PAG [39,40].

The above analysis shows that the adsorption of F^- by PAG consists of two processes: diffusion and adsorption. In the early stage of the adsorption, a large concentration difference produces a great mass transfer capacity, which encourages F^- to migrate to the inner pores of the porous material and bind to

the adsorption sites on the pore walls. In the later stages of adsorption, the slow diffusion of F^- hinders the maximum adsorption potential of the PAG. The fitting results of adsorption kinetics showed that the adsorption process of F^- by PAG was a combination of physical adsorption, chemical adsorption, and ion exchange, which achieved fast and efficient adsorption results.

4 Conclusions

Self-supported porous composites loaded with AFm and AFt were prepared using aluminate cement and flue gas desulfurization gypsum as raw materials by chemical foaming technology. The mineral composition of the adsorbent material prepared from a composite cementitious system consisting of CAC and FGDG was characterized by XRD and SEM. Through the static adsorption experiment, the adsorption effect of the mineral composition of the adsorbent on fluoride ion was deeply analyzed, and the adsorption mechanism was revealed. The conclusions are as follows:

(1) The hydration product phases of the composite cementitious system composed of different proportions of CAC and FGDG are basically the same, mainly AFt, AFm, AH_3, and $CaSO_4{\cdot}2H_2O$.

(2) When the mass ratio of CAC and FGDG was 1:0.2 and 1:0.4, AFm and AH_3 played a major role in adsorption of fluoride ions. When the mass ratio of CAC and FGDG was 1:0.6 and 1:0.7, the main adsorption effect on fluoride ions is AFt, AH_3. When the mass ratio of CAC and FGDG was less than 1:0.7, the adsorption effect on fluoride ions decreased with increasing gypsum admixture. AFt and AFm significantly promote the adsorption effect of fluoride ions.

(3) The isothermal adsorption curves of fluoride ions by the adsorbent materials prepared from the composite cementitious system of aluminate cement and FGD gypsum are in accordance with the Langmuir model. The adsorption process is monolayer adsorption, and the theoretical maximum adsorption capacity is 108.70 mg/g, similar to the measured value of 112.77 mg/g.

(4) The fitting results of adsorption kinetics showed that the adsorption process of F^- by PAG was a combination of physical adsorption, chemical adsorption, and ion exchange, which achieved fast and efficient adsorption results.

Funding Statement: This research was supported by the National Natural Science Foundation of China (No. 52279138). This work was financially supported by Scientific Research Project of Shanxi Province (2018SF-367).

Author Contributions: Xuefeng Song: Writing–original draft, Investigation, Methodology, Formal analysis, Writing–review & editing, Supervision. **Minjuan Sun:** Formal analysis, Writing–review & editing. **Juan He:** Writing–review & editing. **Lei Wang:** Funding acquisition.

Availability of Data and Materials: Data will be made available on request.

Conflicts of Interest: The authors declare that they have no conflicts of interest to report regarding the present study.

References

1. Wei, W., Pang, S. J., Sun, D. J. (2019). The pathogenesis of endemic fluorosis: Research progress in the last 5 years. *Journal of Cellular and Molecular Medicine, 23(4),* 2333–2342. https://doi.org/10.1111/jcmm.14185
2. Yousefi, M., Ghoochani, M., Mahvi, A. H. (2018). Health risk assessment to fluoride in drinking water of rural residents living in the Poldasht city, Northwest of Iran. *Ecotoxicology and Environmental Safety, 148,* 426–430. https://doi.org/10.1016/j.ecoenv.2017.10.057

3. Loganathan, P., Vigneswaran, S., Kandasamy, J., Naidu, R. (2013). Defluoridation of drinking water using adsorption processes. *Journal of Hazardous Materials, 248–249,* 1–19. https://doi.org/10.1016/j.jhazmat.2012.12.043
4. Chinese Center for Disease Control and Prevention (2006). *Standards for drinking water quality.* GB 5749-2006. Beijing: National Health Commission of the People's Republic of China.
5. Li, X., Yuan, Y., Huang, Y., Bi, Z. (2019). Simultaneous removal of ammonia and nitrate by coupled S^0-driven autotrophic denitrification and Anammox process in fluorine-containing semiconductor wastewater. *Science of the Total Environment, 661,* 235–242. https://doi.org/10.1016/j.scitotenv.2019.01.164
6. Chen, Z., Xu, N., Li, W., Zhao, R., Dong, Y. et al. (2019). Effect of trace hydrofluoric acid in a LiPF 6 electrolyte on the performance of a Li-organic battery with an N-heterocycle based conjugated microporous polymer as the cathode. *Journal of Materials Chemistry A, 7(27),* 16347–16355. https://doi.org/10.1039/C9TA01810G
7. Aoudj, S., Khelifa, A., Drouiche, N., Hecini, M. (2016). Removal of fluoride and turbidity from semiconductor industry wastewater by combined coagulation and electroflotation. *Desalination and Water Treatment, 57(39),* 18398–18405. https://doi.org/10.1080/19443994.2015.1095120
8. Carey, M. S., Barsoum, M. W. (2022). Scalable and sustainable production of $Ti_3C_2T_z$ MXene and fluorine recovery from wastewater through cryolite precipitation. *RSC Advances, 12(47),* 30846–30850. https://doi.org/10.1039/D2RA03500F
9. Wan, K., Huang, L., Yan, J., Ma, B., Huang, X. et al. (2021). Removal of fluoride from industrial wastewater by using different adsorbents: A review. *Science of the Total Environment, 773,* 145535. https://doi.org/10.1016/j.scitotenv.2021.145535
10. Grzegorzek, M., Majewska-Nowak, K., Ahmed, A. E. (2020). Removal of fluoride from multicomponent water solutions with the use of monovalent selective ion-exchange membranes. *Science of the Total Environment, 722(3),* 137681. https://doi.org/10.1016/j.scitotenv.2020.137681
11. Nunes-Pereira, J., Lima, R., Choudhary, G., Sharma, P. R., Ferdov, S. et al. (2018). Highly efficient removal of fluoride from aqueous media through polymer composite membranes. *Separation and Purification Technology, 205,* 1–10. https://doi.org/10.1016/j.seppur.2018.05.015
12. Belkada, F. D., Kitous, O., Drouiche, N., Aoudj, S., Bouchelaghem, O. et al. (2018). Electrodialysis for fluoride and nitrate removal from synthesized photovoltaic industry wastewater. *Separation and Purification Technology, 204(3),* 108–115. https://doi.org/10.1016/j.seppur.2018.04.068
13. Tang, J., Chen, Z. L. (2019). Advances in metal-based adsorbent fluoride removal research. *Technology of Water Treatment, 45(11),* 14–18+34. https://doi.org/10.16796/j.cnki.1000-3770.2019.11.003
14. Alhassan, S. I., Huang, L., He, Y., Yan, L., Wu, B. et al. (2021). Fluoride removal from water using alumina and aluminum-based composites: A comprehensive review of progress. *Critical Reviews in Environmental Science and Technology, 51(18),* 2051–2085. https://doi.org/10.1080/10643389.2020.1769441
15. Huang, L., Yang, Z., Zhang, Z., Jin, L., Yang, W. et al. (2020). Enhanced surface hydroxyl groups by using hydrogen peroxide on hollow tubular alumina for removing fluoride. *Microporous and Mesoporous Materials, 297,* 110051. https://doi.org/10.1016/j.micromeso.2020.110051
16. Yang, W., Li, C., Tian, S., Liu, L., Liao, Q. (2020). Influence of synthesis variables of a sol-gel process on the properties of mesoporous alumina and their fluoride adsorption. *Materials Chemistry and Physics, 242,* 122499. https://doi.org/10.1016/j.matchemphys.2019.122499
17. Kumari, U., Behera, S. K., Meikap, B. C. (2019). A novel acid modified alumina adsorbent with enhanced defluoridation property: Kinetics, isotherm study and applicability on industrial wastewater. *Journal of hazardous Materials, 365(1),* 868–882. https://doi.org/10.1016/j.jhazmat.2018.11.064
18. Ghorai, S., Pant, K. K. (2005). Equilibrium, kinetics and breakthrough studies for adsorption of fluoride on activated alumina. *Separation and Purification Technology, 42(3),* 265–271. https://doi.org/10.1016/j.seppur.2004.09.001
19. Yang, K., Li, Y. F., Zhao, Z. J., Tian, Z. L., Lai, Y. Q. (2020). Amorphous porous layered-Al_2O_3 derived from AlFu MOFs as an adsorbent for removing fluorine ions in industrial $ZnSO_4$ solution. *Chemical Engineering Research and Design, 153(1–3),* 562–571. https://doi.org/10.1016/j.cherd.2019.11.019

20. Zhang, Z. J., Tan, Y., Zhong, M. F. (2011). Defluorination of wastewater by calcium chloride modified natural zeolite. *Desalination, 276(1–3),* 246–252. https://doi.org/10.1016/j.desal.2011.03.057
21. Chen, L., He, S., He, B. Y., Wang, T. J., Su, C. L. et al. (2012). Synthesis of iron-doped titanium oxide nanoadsorbent and its adsorption characteristics for fluoride in drinking water. *Industrial & Engineering Chemistry Research, 51(40),* 13150–13156. https://doi.org/10.1021/ie300102v
22. Mukherjee, S., Halder, G. (2018). A review on the sorptive elimination of fluoride from contaminated wastewater. *Journal of Environmental Chemical Engineering, 6(1),* 1257–1270. https://doi.org/10.1016/j.jece.2018.01.046
23. Dutt, M. A., Hanif, M. A., Nadeem, F., Bhatti, H. N. (2020). A review of advances in engineered composite materials popular for wastewater treatment. *Journal of Environmental Chemical Engineering, 8(5),* 104073. https://doi.org/10.1016/j.jece.2020.104073
24. Zhang, G. (2021). *Efficient preparation of chloride ion intercalation LDHs for the nitrate removal from water (Master Thesis)*. Heibei University, China. https://doi.org/10.27103/d.cnki.ghebu.2021.001358
25. Shang, Y. N., Wang, Z. H., Xu, X., Cheng, C., Gao, B. et al. (2019). Enhanced fluoride uptake by bimetallic hydroxides anchored in cotton cellulose/graphene oxide composites. *Journal of Hazardous Materials, 376(6),* 91–101. https://doi.org/10.1016/j.jhazmat.2019.05.039
26. Cai, J. G., Zhao, X., Zhang, Y., Zhang, Q., Pan, B. (2018). Enhanced fluoride removal by La-doped Li/Al layered double hydroxides. *Journal of Colloid and Interface Science, 509(19),* 353–359. https://doi.org/10.1016/j.jcis.2017.09.038
27. Sarma, G. K., Rashid, M. H. (2018). Synthesis of Mg/Al layered double hydroxides for adsorptive removal of fluoride from water: A mechanistic and kinetic study. *Journal of Chemical & Engineering Data, 63(8),* 2957–2965. https://doi.org/10.1021/acs.jced.8b00242
28. Teixeira, M. A., Mageste, A. B., Dias, A., Virtuoso, L. S., Siqueira, K. P. F. (2018). Layered double hydroxides for remediation of industrial wastewater containing manganese and fluoride. *Journal of Cleaner Production, 171,* 275–284. https://doi.org/10.1016/j.jclepro.2017.10.010
29. Yang, C., Xie, Y. Y., Zuo, J. L., Ju, Y. W., Ju, L. T. et al. (2021). Research advances in fluoride removal from water by metal oxides/hydroxides. *Environmental Protection of Chemical Industry, 41(6),* 659–665. https://doi.org/10.3969/j.issn.1006-1878.2021.06.001
30. Xiao, Z. M., Guo, J. P. (2016). Effect of match of specific surface area of cement with gypsum on expansion property of sulpho-aluminate cement and mechanism analysis. *Cement, 10,* 8–10. https://doi.org/10.13739/j.cnki.cn11-1899/tq.2016.10.003
31. Jakob, C., Jansen, D., Ukrainczyk, N., Koenders, E., Pott, U. et al. (2019). Relating ettringite formation and rheological changes during the initial cement hydration: A comparative study applying XRD analysis, rheological measurements and modeling. *Materials, 12(18),* 2957. https://doi.org/10.3390/ma12182957
32. Mesbah, A., Cau-dit-Coumes, C., Renaudin, G., Frizon, F., Leroux, F. (2012). Uptake of chloride and carbonate ions by calcium monosulfoaluminate hydrate. *Cement and Concrete Research, 42(8),* 1157–1165. https://doi.org/10.1016/j.cemconres.2012.05.012
33. Tarali, S. V., Hoolikantimath, N. P., Kulkarni, N., Ghorpade, P. A. (2020). A novel cement-based technology for the treatment of fluoride ions. *SN Applied Sciences, 2(7),* 1205. https://doi.org/10.1007/s42452-020-2986-7
34. Mu, R., Liu, B., Chen, X., Wang, N., Yang, J. (2020). Hydrogel adsorbent in industrial wastewater treatment and ecological environment protection. *Environmental Technology & Innovation, 20,* 101107. https://doi.org/10.1016/j.eti.2020.101107
35. Visa, M. (2016). Synthesis and characterization of new zeolite materials obtained from fly ash for heavy metals removal in advanced wastewater treatment. *Powder Technology, 294(2),* 338–347. https://doi.org/10.1016/j.powtec.2016.02.019
36. Al-Ghouti, M. A., Da'ana, D. A. (2020). Guidelines for the use and interpretation of adsorption isotherm models: A review. *Journal of Hazardous Materials, 393,* 122383. https://doi.org/10.1016/j.jhazmat.2020.122383
37. Ding, P. F., Song, W. F., Wang, C., Yu, Z. F. (2019). Adsorption of Cu(II) and Pb(II) from aqueous solutions onto a metakaolin-based geopolymer. *Desalination and Water Treatment, 158,* 164–173. https://doi.org/10.5004/dwt.2019.24190

38. Najafi, E. K., Arabani, M., Chenari, R. J. (2021). Clay-fly ash geopolymer characterisation and application for the removal of lead and zinc. *Environmental Geotechnics, 40,* 1–12. https://doi.org/10.1680/jenge.20.00065
39. Pongener, C., Bhomick, P. C., Supong, A., Baruah, M., Sinha, U. B. et al. (2018). Adsorption of fluoride onto activated carbon synthesized from *Manihot esculenta* biomass—Equilibrium, kinetic and thermodynamic studies. *Journal of Environmental Chemical Engineering, 6(2),* 2382–2389. https://doi.org/10.1016/j.jece.2018.02.045
40. Gao, Y., You, K., Fu, J., Wang, J., Qian, W. (2022). Manganese modified activated alumina through impregnation for enhanced adsorption capacity of fluoride ions. *Water, 14(17),* 2673. https://doi.org/10.3390/w14172673